Z. Phys. C 72, 239–247 (1996)

ZEITSCHRIFT
FÜR PHYSIK C

Double-β decay of ^{116}Cd

NEMO Collaboration
R. Arnold[10], C. Augier[8], A. Barabash[7], D. Blum[8], V. Brudanin[3], J.E. Campagne[8], D. Dassié[1], V. Egorov[3], R. Eschbach[1], J.L. Guyonnet[10], F. Hubert[1], Ph. Hubert[1], S. Jullian[8], O. Kochetov[3], I. Kisel[3], V.N. Kornoukov[7], V. Kovalenko[3], D. Lalanne[8], F. Laplanche[8,⋆], F. Leccia[1], I. Linck[10], C. Longuemare[2], F. Mauger[2], P. Mennrath[1], H.W. Nicholson[9], A. Nozdrin[3], F. Piquemal[1], O. Purtov[6], J-L. Reyss[4], F. Scheibling[10], J. Suhonen[5], C.S. Sutton[9], G. Szklarz[8], V.I. Tretyak[6], V. Umatov[7], I. Vanushin[7], A. Vareille[1], Yu. Vasilyev[6], Ts. Vylov[3], V. Zerkin[6]

[1] CENBG, IN2P3-CNRS et Université de Bordeaux, F-33170 Gradignan, France
[2] LPC, IN2P3-CNRS et Université de Caen, F-14032 Caen, France
[3] JINR, Dubna, Russia
[4] CFR, CNRS, F-91190 Gif sur Yvette, France
[5] JYVÄSKYLÄ University, FIN-40351 Jyväskylä, Finland
[6] INR, Kiev, Ukraine
[7] ITEP, Moscow, Russia
[8] LAL, IN2P3-CNRS et Université Paris-Sud, F-91405 Orsay, France
[9] MHC, South Hadley, Massachusetts 01075, USA
[10] CRN, IN2P3-CNRS et Université Louis Pasteur, F-67037 Strasbourg, France

Received: 23 May 1996

Abstract. The NEMO-2 tracking detector located in the Fréjus Underground Laboratory was designed as a prototype of the detector NEMO-3 to study 0ν and 2ν double-beta decay ($\beta\beta$) physics. After ten months of nearly continuous running with an enriched cadmium source (0.92 mol·y of ^{116}Cd) a $\beta\beta2\nu$ half-life of $T_{1/2} = (3.75 \pm 0.35(stat) \pm 0.21(syst)) \cdot 10^{19}$ y was measured. Limits with 90% CL on the ^{116}Cd half-lives of $5.0 \cdot 10^{21}$ y for $\beta\beta0\nu$ decay and of $1.2 \cdot 10^{21}$ y for $\beta\beta0\nu\chi^0$ decay with a Majoron (χ^0) were obtained. Theoretical predictions for 0ν and 2ν decays of ^{116}Cd are also presented.

1 Introduction

Several important issues of particle physics, concerning regimes beyond the standard model (SM), can currently be explored most easily by non-accelerator experiments. Particular examples of these modern non-accelerator experiments are the on-going underground experiments concentrating on measurements of the nuclear double beta decay. Measurements of the neutrinoless mode of this decay, $\beta\beta0\nu$, can be used to rule out theoretical models beyond the SM and to limit the possible parameter space of the remaining ones.

The most important observables in the $\beta\beta0\nu$ experiments are the fundamental nature (Dirac or Majorana) and the possible mass of the electron neutrino. These are the key parameters in the structure of modern particle-physics theories, such as GUTs, SUSYs and SUGRAs [1], and are also interesting for their possible role in the matter-antimatter asymmetry of the early universe [2] and in forming the most important component of non-baryonic dark matter in the universe. In addition, the success of models of the solar-neutrino and atmospheric-neutrino deficit strongly depends on assumptions concerning the neutrino masses.

Besides neutrino mass, there are other observables studied in the $\beta\beta0\nu$ experiments which are important for the basic structure of the GUT and SUSY theories. These observables yield information on the mass range of heavy right-handed neutrinos and W_R bosons [3], and thus relate to the group structure of the GUTs. At the same time one can study the feasibility of the exchange of supersymmetric particles in $\beta\beta0\nu$ decays which are allowed by R-parity violating SUSY models [1, 4] and even relate the $\beta\beta0\nu$ experiments to studies of the compositeness of quarks and leptons [5].

One particularly interesting subject of $\beta\beta0\nu$ studies is the Majoron, a light or massless boson which can couple to Majorana neutrinos [6, 7]. The study of the Majoron is useful in pinning down the allowed structures of the GUTs and in solving the solar-neutrino problem. Furthermore, the $\beta\beta0\nu$ measurements can be connected to the possible existence of leptoquarks and heavy sterile neutrinos [8].

All the above mentioned fundamental particle-physics aspects connect to $\beta\beta0\nu$ decay through the evaluation of the associated nuclear matrix elements [9, 10]. The reliability of these matrix elements can be tested in connection with the two-neutrino mode ($\beta\beta2\nu$) of double-beta decay. The measured $\beta\beta2\nu$ half-lives and the simple phase-space structure of the $\beta\beta2\nu$ decay allow a straight forward extraction of the experimental value of the associated double Gamow–Teller (DGT) matrix element. This extracted value can be compared with theoretical predictions, obtained for medium-heavy and heavy nuclei by several theory groups using the proton-neutron quasiparticle random-phase approximation (pnQRPA) and its various extensions [11]-[17]. Per-

⋆ (e-mail: laplanche@lalcls.in2p3.fr, Fax: (33) 1 69 07 94 04)

forming such studies helps in reducing the uncertainties involved in the nuclear-structure part of the various $\beta\beta0\nu$ processes. The theoretical results of the present article are obtained by using the pnQRPA [18] in the framework of reference [10].

To date, only lower limits on half-lives of different nuclei for $\beta\beta0\nu$ decay have been obtained experimentally. The most stringent limit was obtained for ^{76}Ge, $T^{0\nu}_{1/2} > 5.1 \cdot 10^{24}$ y [19], corresponding to the limit $m_\nu < (0.7 - 1.7)$ eV on the Majorana-neutrino mass. Up to the present, the $\beta\beta2\nu$ decay process has been detected for eight nuclei (see review [20]). Also the $\beta\beta2\nu$ decay of ^{100}Mo to the first 0^+ excited state in ^{100}Ru has been measured [21]. At present, the $\beta\beta2\nu$ experiments are achieving a new qualitative level, where it is not enough just to detect the process, but it is necessary to measure all parameters (angular correlation, single electron spectra, ...) of the process with good accuracy.

The NEMO Collaboration has started to build the tracking detector NEMO-3 [22] for $\beta\beta$ decay experiments which will be capable of studying $\beta\beta0\nu$ decays of ^{100}Mo and others nuclei up to half-lives $\sim 10^{25}$ y, which corresponds to a Majorana neutrino mass $\sim$ 0.1 to 0.3 eV. Sensitivity to $\beta\beta0\nu\chi^0$ and $\beta\beta2\nu$ decays will be $\sim 10^{23}$ y and $\sim 10^{22}$ y, respectively. Two prototype detectors, NEMO-1 [23] and NEMO-2 [24] have been constructed as research and development tools to establish reliable techniques. The NEMO-2 detector, designed for $\beta\beta$ and background studies, is currently operating in the Fréjus Underground Laboratory (4800 m w.e.). During a period from 1992 into 1993 ^{100}Mo was investigated by this detector. $\beta\beta2\nu$ decay of ^{100}Mo was detected by measuring the summed energy spectra, angular distribution and single electron spectra [25]. Presented here are the results of measurements with ^{116}Cd, which is one of the most favourable nuclides ($Q_{\beta\beta}$ = 2802 keV) in the search for $\beta\beta$ processes.

2 NEMO-2 detector

NEMO-2 consists of a 1m^3 tracking volume filled with helium gas and 4% ethyl alcohol.

Vertically bisecting the detector is the plane of the source foil (1m $\times$ 1m). Tracking is accomplished with long open Geiger cells with an octagonal cross section defined by 100 μm nickel wires. These cells are identical to those of NEMO-1. On each side of the source foil there are 10 planes of 32 cells which alternate between vertical and horizontal orientations. The cells provide three-dimensional tracking of charged particles.

A calorimeter made of scintillators covers two vertical opposing sides of the tracking volume. There have been two configurations of the calorimeter, the first consisted of two planes of 64 scintillators (12 cm$\times$12 cm$\times$2.25 cm) associated with "standard" photomultiplier tubes (PMTs). The present configuration is two planes of 25 scintillators (19 cm$\times$19 cm$\times$10 cm) with PMTs made of low radioactivity glass. The tracking volume and scintillators are surrounded with a lead (5 cm) and iron (20 cm) shield.

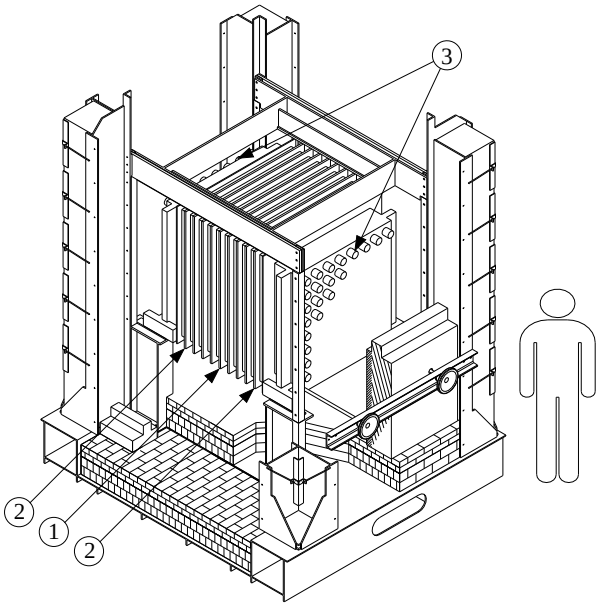

Fig. 1. The NEMO-2 detector without shielding. (1) Central frame with the source plane capable of supporting plural source foils. (2) Tracking device of 10 frames, each consisting of two perpendicular planes of 32 Geiger cells. (3) Two scintillator arrays each consisting of 5 by 5 counters. In the earlier experiment with molybdenum sources the scintillator arrays were 8 by 8 counters as depicted here

2.1 Cadmium sources

The source plane is divided into two halves, the first is a 152 g isotopically enriched cadmium foil (93.2% is ^{116}Cd) with a thickness of 40μm. The second half is a 143 g foil of natural cadmium of which 7.49% is ^{116}Cd. Radioactive impurities in both foils were measured with HPGe detectors in the Fréjus Underground Laboratory before installation in the NEMO-2 detector. The upper limits (90% C.L.) on the measured contaminations obtained in the enriched cadmium foil for the three most disturbing isotopes ^{214}Bi, ^{208}Tl and ^{234m}Pa are 2, 2, and 66 mBq/kg respectively. In the natural cadmium these limits are 1.7, 2.5 and 33 mBq/kg. More accurate levels have been obtained with the NEMO-2 detector by analyzing electron events involving γ rays, as explained in the sections devoted to backgrounds. The above contamination limits, if taken as levels, will only produce a very few "two-electron" events in each foil.

2.2 Performances

The achieved performances and operating parameters are as follows. Three-dimensional measurements of charged particle tracks are provided by the array of Geiger cells. The transverse position is given by the drift time and the longitudinal position by the plasma propagation times. The transverse resolution is 500 μm and the longitudinal resolution is 4.7 mm. Track reconstruction is accomplished with a pattern recognition program based on the Kalman filter [26]. A new tracking method based on an elastic neural network [27] was used to test the tracking efficiency. Given the cuts of the $\beta\beta2\nu$ analysis, both methods gave the same half-life calculations.

The threshold for the scintillators is set at 50 keV with an energy resolution (FWHM) of 18% at 1 MeV and a time resolution of 275 ps (550 ps at 0.2 MeV). A laser and fiber optics device is used to check the stability of the scintillation detectors, this device also provides the time versus charge dependence of the detectors. The relative timing offsets for each channel were determined with a ^{60}Co source placed in the center of the detector.

A trigger requiring two scintillation counters and four Geiger frames normally runs at a rate of 0.01-0.04 Hz depending on the radon levels in the laboratory. This trigger rate is too low for an efficient survey of the experiment, so a second trigger requiring only one counter with an energy greater than 1.3 MeV was introduced to yield a rate of 0.4-0.8 Hz. This trigger conveniently records single electron events.

Finally, the NEMO-2 detector is able to measure the internal radioactive contamination of the foils by using the electron gamma (eγ) and (e$\gamma\alpha$) channels where a delayed α detection is a signature of ^{214}Bi decaying into ^{214}Po with a half-life of 164 μs.

2.3 Event definition

An electron is defined by a track linking the source foil and one scintillator. The maximum scattering angle along the track has to be less than 20° to reject hard scattering situations. A photon is recognized as one or two adjacent fired scintillators without an associated particle track. For photons and electrons an energy deposited greater than 200 keV is required in order to obtain sufficiently good time resolution. In the analysis of two-electron events a cut on the angle between the two electron tracks will be applied (cos $\alpha < 0.6$) as explained in the section devoted to the results. In the analysis a two-electron event is identified as (2e) and electron-photon event as (eγ).

In the coordinate system of the detector (Fig. 5) the origin of the axes is at the center of the source plane with the x axis being horizontal and the y axis vertical. The positioning of the enriched cadmium foil is such that it has an event vertex x coordinate in the range 1.0 to 47.5 cm. Both foils are symmetrical with respect to the y axis. The event y vertex has to be within the limits $\pm$47.5 cm.

3 Backgrounds

The most important "external" background is due to photons originating from outside of the tracking detector and interacting with the source foils or with the scintillators. Compton electrons produced in the scintillators and crossing the tracking device are rejected by time-of-flight analysis. Compton electrons produced in the source foils can generate a secondary electron by the Möller effect. A double Compton effect or pair production can also occur. These 2e background events cannot be rejected by time-of-flight cuts.

Radioactive pollution of the source foils is a background identified as "internal". A beta electron which gives rise to the Möller effect or is associated with an internal conversion electron or is associated with a Compton electron can produce 2e background events. Another source of background originates from neutron capture in natural cadmium which produces photon emissions. All these backgrounds are studied below and their contributions to the $e\gamma$ and 2e channels are identified.

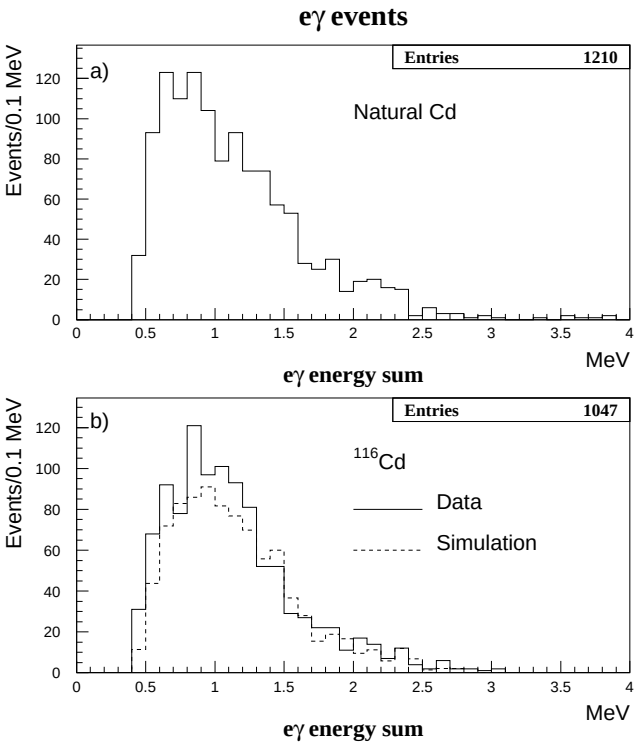

Fig. 2. In natural cadmium **(a)** the greater number of events with respect to enriched cadmium is explained by the internal background and by neutron capture in ^{113}Cd. The simulated energy spectrum (dotted line) which only takes into account the two major sources of external background i.e., radon and PMT's radioactivity, reproduces quite well the shape of the experimental spectrum in enriched cadmium **(b)**

3.1 External background

The most important contribution to the external background comes from the flux of photons emitted by radon located between the tracking detector and the shielding. The mean value of the measured radon rate in the laboratory was 27 ± 10 Bq/m^3 during data collection, with large fluctuations depending on the ventilation. A simulation of the photons coming from ^{214}Bi decay (produced in the cascade) yields somewhat more than one half of the detected eγ events.

Another source of background is due to the flux of photons emitted by the PMT's glass, this effect is much weaker than in the previous experiment [25] because of the low activity of the current PMTs. The measured activity of samples of these tubes has given the following results: 0.23 Bq/kg of ^{214}Bi, 1.5 Bq/kg of ^{40}K and 0.043Bq/kg of ^{208}Tl. A simulation, using these values, shows that the eγ events attributed to the PMT's glass represent about one quarter of the total eγ events.

A run time equivalent simulated spectrum, using only these two sources of background, i.e., radon and the PMT's components, is compared to the experimental data in Fig. 2.

The energy sum spectrum for eγ events shows that the simulation reproduces rather well the experimental data in the enriched cadmium foil. The excess of events in natural cadmium, compared to enriched cadmium, is attributed to internal pollution and to thermal neutron capture as explained in the following sections.

The 2e events obtained in the simulations have too poor statistics to be used as a good estimate of the 2e background. This is because the number of simulated events was reduced to a reasonable computing time, and the eγ spectrum was renormalized. A precise estimate of this background is achieved using the 2e experimental events in the natural cadmium foil.

3.2 Thermal neutron capture

The thermal neutron capture cross-section in ^{113}Cd (12.22% of natural cadmium) is huge (20000 barn). A capture is followed by the emission of photons coming from the de-excitation of ^{114}Cd. The neutron flux in the laboratory or inside the detector is not well known, so a simulation would not give a reliable estimate of its effect. A short run (6.2 h) with an Am-Li neutron source placed inside a moderator on the top of the shielding has given eγ and 2e events mainly due to thermal neutrons.

In Fig. 3 the 2e events recorded during the neutron run are presented and the 2e energy sum is plotted versus cos α. A clear excess of events in the natural cadmium is the signature of thermal neutron captures in ^{113}Cd. Four of the 2e events remain after the cuts of the $\beta\beta2\nu$ analysis (Fig. 3–a).

As neutron capture in materials surrounding the tracking detector induces a photon flux, a normalization can be done using Compton electrons produced in the scintillator which cross the detector and lose their energy in another scintillator. Only events with an energy deposited greater than 4 MeV were used in this normalization. The neutron run is found to be equivalent in total exposure to twice the 6588 h run. Thus an excess of 38 eγ events and two 2e events in natural cadmium is deduced, which is attributed to the thermal neutron flux inside the detector.

3.3 Internal background

The above measurements of the cadmium source foils with germanium detectors gave upper limits on the ^{214}Bi, ^{208}Tl and ^{234m}Pa contaminations. The NEMO-2 detector itself provides limits and/or measurements of foil activities by analysing eγ, e$\gamma\alpha$ and single electron events. In the natural and in the enriched cadmium foils ^{214}Bi activities of 2.5 ± 0.5 mBq/kg and 1.5 ± 0.5 mBq/kg have been found (the dominant systematic error is due to radon which enters the detector and is deposited on both foils). An excess of 1 ± 0.5 mBq/kg is measured in the natural cadmium which induces 50 eγ events and 2.2 2e events. These event rates were obtained by simulations which take into account accurate representations of nuclear decay schemes.

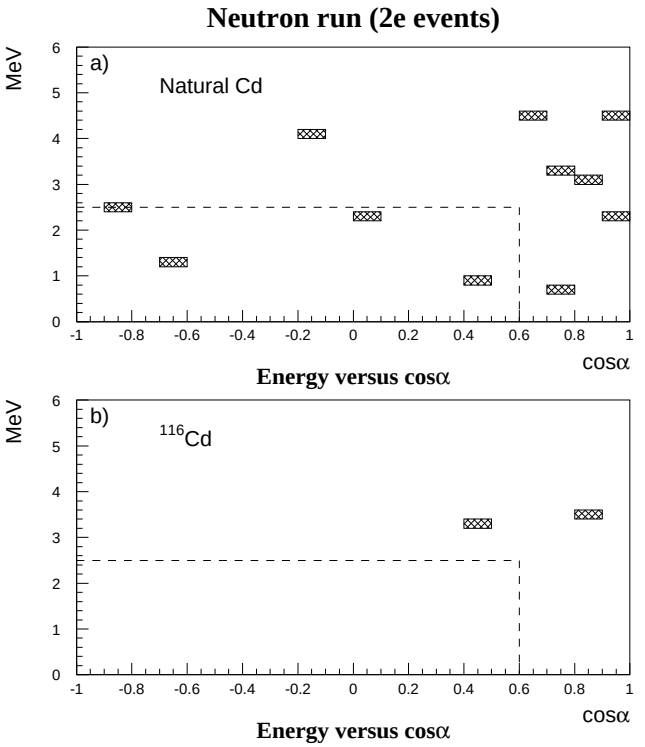

Fig. 3. These scatter plots extracted from the neutron run of 6.2 h (Am-Li source in a moderator) clearly show an excess of 2e events in the natural cadmium **(a)** with respect to enriched cadmium **(b)**, due to neutron capture in ^{113}Cd. Inside the rectangular region outlined by the dashed lines is the parameter space of selected 2e events

In order to measure the ^{208}Tl contamination, the high energy tail (2.0 to 2.5 MeV) of the photon spectrum of eγ events was used. In the enriched cadmium foil which is not affected by neutron capture, a limit of 0.5 mBq/kg is computed which corresponds to less than 1.5 2e events. In the natural cadmium foil, the photon spectrum in the 2.5 MeV region is expected to be populated by some events induced by neutron capture. By using the normalized neutron run to estimate this background, an upper limit of 1 mBq/kg is calculated for the ^{208}Tl contamination.

Another source of background in the 2e channel comes from ^{234m}Pa and/or ^{90}Sr which are single beta emitters. Using the single electron energy spectra in the range $1.5 \leq E_{el} \leq 2.0$ MeV, limits on the contamination can be calculated in both foils. The same counting rates were found in the natural and in the enriched foils. The radon contribution was eliminated by analyzing data with different radon rates in the laboratory, and a limit of 28 mBq/kg is deduced in each foil. The limit on the difference of contamination in both foils of 6 mBq/kg is obtained which corresponds to less than 4.5 2e events.

In Fig. 4 the single electron energy spectra of natural and enriched cadmium are shown for 10% of the complete data set. The simulated spectrum corresponding to 28 mBq/kg of ^{243m}Pa is also included in the figure for comparison of spectra profiles.

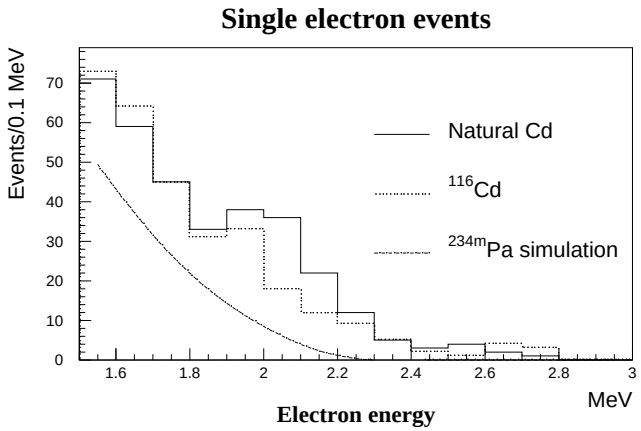

Fig. 4. Single electron energy spectra are used to place limits on the ^{234m}Pa contamination. By analyzing the spectra in the energy range 1.5 to 2.0 MeV (for 10% of the complete data set) a limit of 28 mBq/kg is calculated in each foil. In the experimental spectra within the energy range defined above 40% of the events are attributed to the effect of radon. A limit on the statistical difference of contamination between the foils of 6 mBq/kg is computed

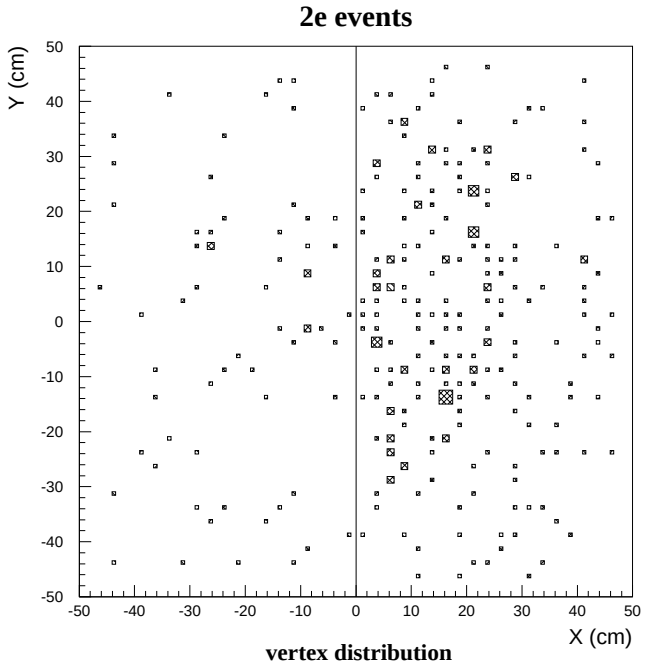

Fig. 5. Evidence of an excess of events in enriched cadmium (right half) is shown in this scatter plot. In each source the non-uniformity of the vertex distribution is due to the geometric acceptance of the detector

4 Results

An earlier result, drawn from 40% of the current data set, has already been published [28].

4.1 $\beta\beta2\nu$ signal

The 2e events are defined by two tracks with a common vertex associated with two fired scintillators and a deposited energy of at least 200 keV in each one. In the first step the 2e events are selected by time-of-flight analysis. For each event the probability of it being an internal (P_{int}) or an external (P_{ext}) source event are computed. By applying the cuts $P_{int} > 10^{-2}$ and $P_{ext} < 10^{-5}$ very few background events are expected in each foil. The complete cadmium data set (6588 h of running time) is presented here.

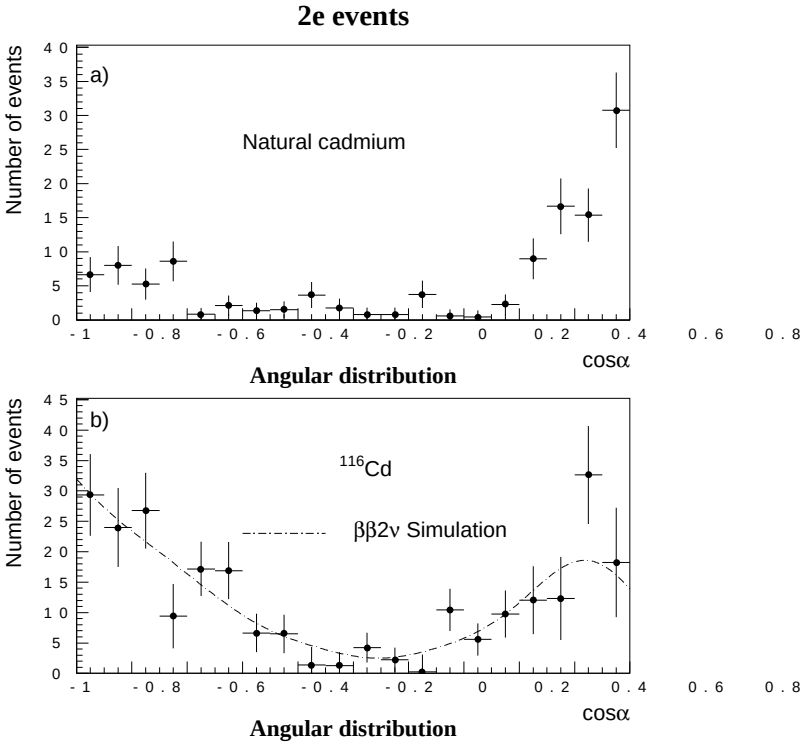

Fig. 6. The angular distribution in the natural cadmium foil **(a)**, where α is the angle between the two electron tracks, is peaked in the forward direction as expected from the external photon flux. A scaled estimate of the $\beta\beta2\nu$ decay contribution, in accordance with the ^{116}Cd abundance in natural Cd has been subtracted. The angular distribution in enriched cadmium **(b)** after background subtraction is in good agreement with the simulation

The vertex distribution (Fig. 5) in the source plane shows a clear excess of 2e events in the enriched cadmium (positive X-positions).

The distributions of the angle between the two emitted electrons in enriched cadmium with backgrounds subtracted (Fig. 6-a) and in natural cadmium (Fig. 6-b) are rather different.

In the natural cadmium, the angular distribution is peaked in the forward direction, as expected from the external background. After background subtraction the cos α distribution in enriched cadmium is in agreement with the simulation of a pure $\beta\beta2\nu$ decay spectrum. (Fig. 6-b). The 2e background in the enriched cadmium foil is evaluated by using 2e events in the natural cadmium foil.

In order to improve the signal to background ratio the cut cos $\alpha \leq 0.6$ is applied in the selection of 2e events. The raw data energy spectra in enriched cadmium (220 events) and in natural cadmium (61 events) are shown in Fig. 7.

The useful energy range for $\beta\beta2\nu$ decay in this experiment is limited to 2.5 MeV, then the number of events used for a half-life calculation is 219 in enriched cadmium and 58 in natural cadmium with a $\beta\beta2\nu$ contribution of 13.6 events (assuming $T_{1/2} = 3.75 \cdot 10^{19}$ y).

Estimates of 2e events induced by internal background were made in the previous section, leading to an excess of

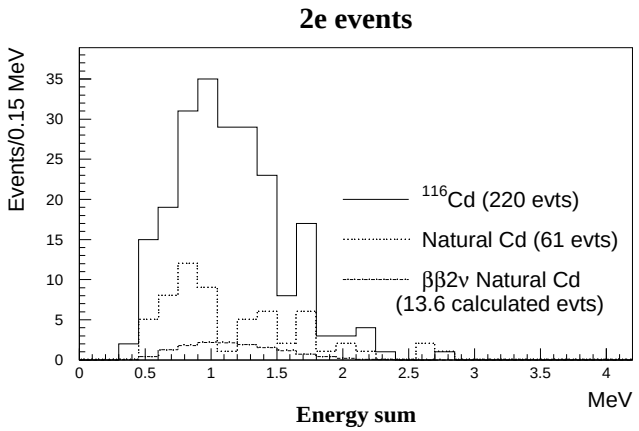

Fig. 7. The raw data energy spectra before background subtraction in enriched cadmium (solid line) and in natural cadmium (dotted line) are shown here. The corresponding $\beta\beta2\nu$ spectrum contribution in natural cadmium is also represented (dashed-dotted line). Only one event in enriched cadmium is found in the 2.4 - 3 MeV energy range. (The end point energy $Q_{\beta\beta}$ = 2.802 MeV)

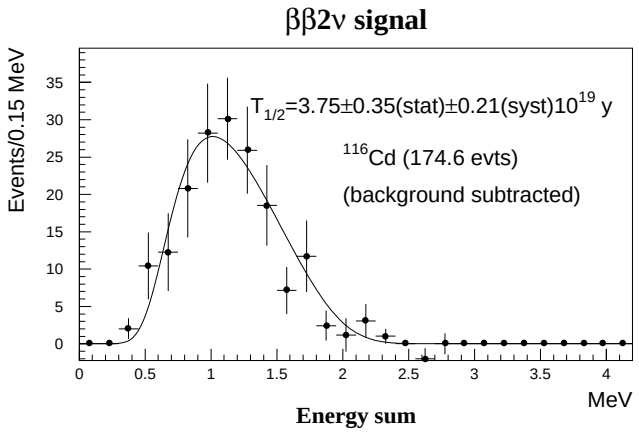

Fig. 8. Summed electron energy spectrum of $\beta\beta2\nu$ events in ^{116}Cd. The solid line represents the simulated spectrum for a half-life of $3.75 \cdot 10^{19}$ y

4.2 events in natural cadmium. Another cause for the small variation between the two foils is due to their difference in thickness which gives an excess of 5 ± 1 2e events in the enriched foil induced by the external photon flux. This last effect compensates for the excess mentioned above. Finally the 2e background measured in natural cadmium (experimental 2e events minus the computed $\beta\beta2\nu$ contribution) is used to subtract the 2e background in enriched cadmium.

The $\beta\beta$ energy spectrum in enriched cadmium (174.6 events) is obtained after background subtraction (44.4 events) and compared to the simulation in Fig. 8.

Using the Monte Carlo calculated detection efficiency for the $\beta\beta2\nu$ decay of ^{116}Cd (ε = 1.73%) one gets,

$$T^{2\nu}_{1/2} = [3.75 \pm 0.35(stat) \pm 0.21(syst)] \cdot 10^{19} y$$

The main contributions to the systematic error are due to the Monte-Carlo calculations, energy calibration, thermal neutron flux, internal and external background subtractions.

The error in the efficiency calculations which is due to the uncertainty in the simulated electron scattering angle has been estimated to be 3%, a factor of two better than in

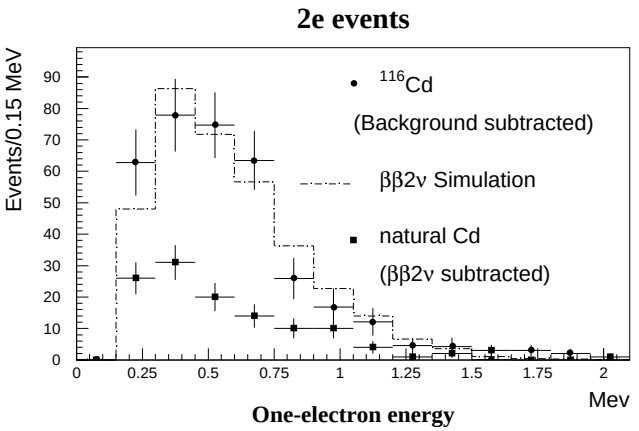

Fig. 9. The one-electron energy distribution in ^{116}Cd is reproduced by the simulation using the measured half-life of $3.75 \cdot 10^{19}$ y . In natural cadmium the $\beta\beta2\nu$ contribution has been subtracted. (In both spectra there are two entries per event)

the ^{100}Mo analysis. In the new simulation (GEANT 3.21) the step size, which is the most important parameter, was optimized by a large increase in computational power.

Next the absolute error in the energy calibration for 200 keV electrons is 10 keV. Thus, using the one-electron energy spectrum (Fig. 9), one deduces a systematic error of 3% induced by this calibration.

The only measurement of internal background was made for ^{214}Bi. If the limits obtained for ^{208}Tl and ^{234m}Pa are taken as measurements, a systematic error in the internal background subtraction of 3% is calculated. This error is improved by a factor of 2 with respect to the previous experiment with molybdenum. As estimated above, the thermal neutrons in the detector induce two 2e events which have a 1% effect on the signal.

Finally using the difference in the numbers of eγ events in both foils (after the internal background and the neutron effect are subtracted) and the calculated 2e external background in natural cadmium (44.4 events), a systematic error in the external background subtraction of 2% is obtained. This error when compared to the molybdenum experiment is again reduced by a factor of two. Finally a total systematic error of 5.5% is affixed to the half-life.

4.2 Limits on 0ν modes

Monte Carlo simulations of the summed electron energy spectrum are shown in Fig. 10 for $\beta\beta0\nu$ decays to the ground state, with and without Majoron emission, and for decays to the excited 2^+ state (1293.5 keV).

Half-life limits extracted from the data are given in Table 1.

The energy windows, number of events, backgrounds, and efficiencies are also given. Limits are computed with the formula for Poisson processes with background [29].

5 Theoretical predictions

In this work the $\beta\beta2\nu$ and $\beta\beta0\nu$ decays are analyzed by the pnQRPA [18] and the $\beta\beta0\nu$ framework of [10]. The calcu-

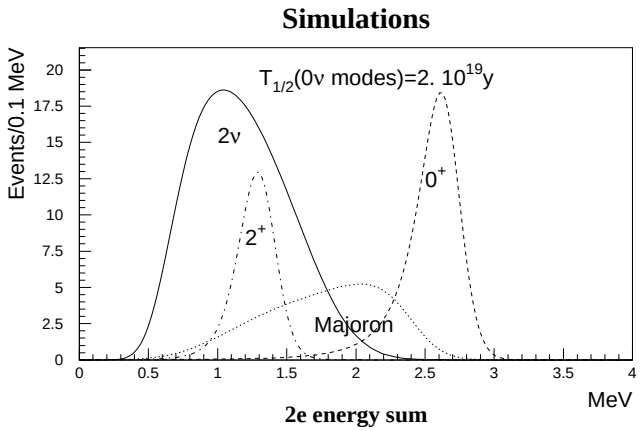

Fig. 10. $\beta\beta$ decay spectra used in computing the corresponding limits. Here the 0ν modes are plotted for half-lives of $2 \cdot 10^{19}$ y. The curves for the different modes explain the energy windows used in Table 1

Table 1. Half-life limits (90% C.L.). For each decay channel an energy window is defined, the corresponding number of experimental events, the number of calculated $\beta\beta2\nu$ events, the efficiency, and the half-life limit are given

Channel	$0^+_{\rm g.s.}$	Majoron	2^+
Window (MeV)	[2.4,3.0]	[1.8,2.55]	[1.2,1.5]
Number of events	1	11	52
Background $+\beta\beta2\nu$	3.2	12.2	54
Efficiency (%)	3.7	1.8	1.8
$T_{1/2}(10^{21}$ y)	$>$5.0	$>$1.2	$>$0.6

lations have been performed using 16 single-particle orbitals for both protons and neutrons. Realistic two-body interaction matrix elements [18] were used in the calculations.

A transformation from particles to quasiparticles was made by the use of the BCS theory [18]. A comparison between the BCS quasiparticle energies and the low-energy spectra of the relevant odd-proton and odd-neutron nuclei was made. A slight adjustment of the proton and neutron single-particle energies near the Fermi surface was carried out to improve the correspondence between the experimental and theoretical one-quasiparticle spectra. The scaling of the strength of the pairing channel and the proton–neutron 1^+ channel was done according to [18] by comparing the predicted lateral beta-decay feeding of ^{116}Cd and ^{116}Sn, both by β^- and β^+/EC transitions, with available data.

After these procedures the double beta matrix elements are predicted and the DGT matrix element can be compared with the present new experimental data on $\beta\beta2\nu$ decay of ^{116}Cd. The calculated $\beta\beta2\nu$ half-life, $T^{2\nu}_{1/2} = 5.15 \cdot 10^{19}$y is rather close to the extracted experimental value $T^{2\nu}_{1/2} = 3.75 \cdot 10^{19}$y and thus would indicate that the two-body matrix elements are properly scaled.

The next theoretical step was to construct the wave functions of the other intermediate J^π states and to evaluate the various $\beta\beta0\nu$ matrix elements according to [10]. In the formalism of [10] the $\beta\beta0\nu$ half-life can be written in the form

Table 2. The values of the half-life coefficients of Eq. (1) for the ^{116}Cd decay

Coefficient	$C^{(0)}_{mm}$	$C^{(0)}_{\lambda\lambda}$	$C^{(0)}_{\eta\eta}$
Value [y^{-1}]	$6.61 \cdot 10^{-13}$	$1.55 \cdot 10^{-12}$	$2.28 \cdot 10^{-8}$
Coefficient	$C^{(0)}_{m\lambda}$	$C^{(0)}_{m\eta}$	$C^{(0)}_{\lambda\eta}$
Value [y^{-1}]	$-4.05 \cdot 10^{-13}$	$1.05 \cdot 10^{-10}$	$-9.35 \cdot 10^{-13}$

$$\left(T^{0\nu}_{1/2}\right)^{-1} = C^{(0)}_{mm}\left(\frac{\langle m_\nu\rangle}{m_{\rm e}}\right)^2 + C^{(0)}_{\lambda\lambda}\langle\lambda\rangle^2 + C^{(0)}_{\eta\eta}\langle\eta\rangle^2$$
$$+C^{(0)}_{m\lambda}\left(\frac{\langle m_\nu\rangle}{m_{\rm e}}\right)\langle\lambda\rangle + C^{(0)}_{m\eta}\left(\frac{\langle m_\nu\rangle}{m_{\rm e}}\right)\langle\eta\rangle + C^{(0)}_{\lambda\eta}\langle\lambda\rangle\langle\eta\rangle \ . \qquad (1)$$

where the $C^{(0)}$ coefficients of (1) contain information about the phase space and nuclear matrix elements. The present values of the $C^{(0)}$ coefficients are listed in Table 2

By using (1) and the experimental half-life limit, $T^{0\nu}_{1/2} > 5.0 \cdot 10^{21}$y, the following upper limits for the effective neutrino mass and right-handed coupling strengths: $|\langle m_\nu\rangle| <$ 9.8 eV, $|\langle\eta\rangle| < 10.3 \cdot 10^{-8}$, $|\langle\lambda\rangle| < 1.13 \cdot 10^{-5}$ were derived. At the same time, the s-wave matrix element $M^{(s)}_m$ [10] was used to deduce an upper limit for the effective Majoron-Majorana neutrino coupling strength, $\langle g_{\rm M}\rangle$, by using the following half-life formula [9, 37] for Majoron emission

$$\left(T^{0\nu{\rm M}}_{1/2}\right)^{-1} = |\langle g_{\rm M}\rangle|^2\left(M^{(s)}_m\right)^2 G_{\rm B} \ , \qquad (2)$$

where $G_{\rm B} = 2.23 \cdot 10^{-13}{\rm fm}^2{\rm y}^{-1}$ is the phase-space integral for Majoron emission. Finally, using the experimental half-life limit, $T^{0\nu{\rm M}}_{1/2} > 1.2 \cdot 10^{21}$y, the calculated value of $M^{(s)}_m$ (389 in $m_e c^2$ unit) and the above half-life equation, one deduces the upper limit $|\langle g_{\rm M}\rangle| < 1.2 \cdot 10^{-4}$ for the Majoron-Majorana coupling.

6 Discussion

Some recent results are recalled here for comparison. Using an enriched crystal scintillator [30] a half-life $T_{1/2} = [2.7^{+0.5}_{-0.4}(stat)^{+0.9}_{-0.6}(syst)] \cdot 10^{19}$ y was published with the restriction that ^{90}Sr impurities imitating the effect cannot be excluded. Another result from the ELEGANT V detector [31] gives the half-life $T_{1/2} = [2.6^{+0.9}_{-0.5}] \cdot 10^{19}$ y which is very close to the previous one. But in this experiment one also cannot exclude the effect of ^{90}Sr. The corresponding $\beta\beta0\nu$ decay mode to the ground state gives the following experimental limits: $T^{0\nu}_{1/2} > 2.9 \cdot 10^{22}$ y (90% CL) [1] [30] and $T^{0\nu}_{1/2} > 2.9 \cdot 10^{21}$ y (90% CL) [31]. The decay into the 1293.5 keV excited state (2^+) has been investigated by another experiment using an external source with a Ge detector [32] leading to $T^{0^+\to2^+}_{1/2} > 2.37 \cdot 10^{21}$ y (90% CL).

The present theoretical estimates for the $\beta\beta2\nu$ and $\beta\beta0\nu$ matrix elements are based on fixing the magnitudes of the two-body interaction matrix elements with various data, not

[1] Following the technique recommended by Particle Data Group [29] the limit is $6 \cdot 10^{21}$ at 90% CL

directly connected to $\beta\beta$ decay. This data includes the quasiparticle spectra of the relevant odd-proton and odd-neutron nuclei, proton and neutron separation energies, Gamow–Teller giant resonance in ^{116}In and, finally, the data on lateral beta-decay feeding of ^{116}Cd and ^{116}Sn. This leaves the $\beta\beta$ observables as pure predictions, subject to critical comparison with the present $\beta\beta2\nu$ data. It is found that the theoretical $\beta\beta2\nu$ half-life compares quite well with the experimental one. At present, the $\beta\beta0\nu$ matrix elements cannot be directly compared with data, so that comparison with other calculations remains the only method of controlling their values.

The magnitude of the present $\beta\beta2\nu$ DGT matrix element is twice the one reported in reference [32]. This is due to two reasons. The first is that in the present calculation the above-mentioned philosophy of using the single beta decay data in pinning down the magnitude of the proton-neutron two-body matrix elements is adopted. In [32] the bare G-matrix was used in the calculations. Secondly in the present calculation the single-particle energies have been adjusted in the vicinity of the proton and neutron Fermi surfaces. In [32] this procedure was not used.

The predicted $C^{(0)}$ coefficients can be compared with the ones of [14]. All the coefficients have practically the same value in these two calculations, except $C^{(0)}_{m\eta}$ and $C^{(0)}_{\eta\eta}$ which are factors of 1.5 and 1.9 bigger, respectively, in the present calculation. The agreement between these two calculations is surprisingly good considering that in [14] the two criteria, mentioned in the previous paragraph, were not used. This indicates that the values of the $\beta\beta0\nu$ matrix elements are less dependent on the single-particle basis and fine details of the two-body interaction than the $\beta\beta2\nu$ matrix elements. This is a convenient feature since it reduces theoretical uncertainties and, in the present case, seems to lead to rather small systematic errors in the predicted upper limits for the neutrino mass and right-handed coupling parameters. One further observation, concerning the $C^{(0)}_{\eta\eta}$ coefficient, is that the so-called p-wave effect [9], mediated by the M_{P} matrix element [10], is in this case very small, of the order of 1 per cent.

One can compare the present upper limits of the effective electron neutrino mass and the right-handed coupling strengths with the corresponding values coming from theoretical estimates for other $\beta\beta0\nu$ decaying nuclei. The present upper limits for $\langle m_\nu\rangle$, $|\langle\lambda\rangle|$ and $|\langle\eta\rangle|$ cannot compete with the ones extracted from the ^{128}Te [33], ^{76}Ge [19] and ^{136}Xe [34] experiments. The present upper limit for the Majoron-Majorana neutrino coupling constant, $|\langle g_{\mathrm{M}}\rangle| < 1.2 \cdot 10^{-4}$, is of good quality when compared to results coming from other counter experiments [20, 34, 35, 36, 37]. One of the best limits can be extracted from the ^{150}Nd experiment ($T_{1/2} > 5.3 \cdot 10^{20}$ y, [35]). Using the nuclear matrix element from [14] the limit $|\langle g_{\mathrm{M}}\rangle| < 0.7 \cdot 10^{-4}$ can be obtained, but using the latest nuclear matrix element calculations for ^{150}Nd [38] the limit is $3.8 \cdot 10^{-4}$. Only the geochemical data on ^{128}Te decay yields a more constraining limit, $|\langle g_{\mathrm{M}}\rangle| < (3 - 7.8) \cdot 10^{-5}$ [33, 37] if one uses the experimental result [33]. Alternatively if one uses the results of two other experiments [39, 40] the limit will be $|\langle g_{\mathrm{M}}\rangle| < (0.6 - 1.5) \cdot 10^{-4}$.

7 Conclusion

After the first experiment with enriched molybdenum which showed the capabilities of the NEMO-2 detector, a second experiment with an improved calorimeter (low background PMTs and thicker scintillators) has generated double-beta decay measurement of an enriched cadmium source. The systematic error on the $\beta\beta2\nu$ half-life was of 9.5% in the first experiment and was lowered to 5.5% in the present one. In both experiments a very low background is measured in the expected $\beta\beta0\nu$ decay energy region. New sources of enriched selenium and zirconium were installed in NEMO-2 (autumn 1995) and data collection has started. The NEMO-3 detector is currently under construction and will be installed in the Fréjus Underground Laboratory in 1998.

Acknowledgements. The authors would like to thank the Fréjus Underground Laboratory staff for their technical assistance in running the experiment.

References

1. R. N. Mohapatra and P. B. Pal: Massive Neutrinos in Physics and Astrophysics (World Scientific, Singapore, 1991)
2. M. Fukugita and T. Yanagida: Phys. Rev. D42 (1990) 1285
3. J. D. Vergados: Phys. Reports 133 (1986) 1
4. M. Hirsch, H. V. Klapdor-Kleingrothaus and S. G. Kovalenko: Phys. Rev. Lett. 75 (1995) 17
5. E. Takasugi: in Proc. of the International Workshop on Double Beta Decay and Related Topics, Trento, April 24 – May 5, 1995, eds. H. V. Klapdor-Kleingrothaus and S. Stoica (World Scientific, Singapore), p. 165
6. Z. G. Berezhiani, A. Yu. Smirnov and J. W. F. Valle: Phys. Lett. B291 (1992) 99
7. C. P. Burgess and J. M. Cline: Phys. Lett. B298 (1993) 141 ; Phys. Rev. D49 (1994) 5925
8. R. N. Mohapatra: in Proc. of the International Workshop on Double Beta Decay and Related Topics, Trento, April 24 – May 5, 1995, eds. H. V. Klapdor-Kleingrothaus and S. Stoica (World Scientific, Singapore), p. 44
9. M. Doi, T. Kotani and E. Takasugi: Prog. Theor. Phys. Suppl. 83 (1985) 1
10. J. Suhonen, S. B. Khadkikar and A. Faessler: Phys. Lett. B237 (1990) 8 ; Nucl. Phys. A529 (1991) 727 ; *ibid.* A535 (1991) 509
11. P. Vogel and M. R. Zirnbauer: Phys. Rev. Lett. 57 (1986) 3148
12. O. Civitarese, A. Faessler and T. Tomoda: Phys. Lett. B194 (1987) 11
13. K. Muto, E. Bender and H. V. Klapdor: Z. Phys. A334 (1989) 177 ; *ibid.* A334 (1989) 187
14. A. Staudt, K. Muto and H. V. Klapdor-Kleingrothaus: Europhys. Lett. 13 (1990) 31
15. O. Civitarese, A. Faessler, J. Suhonen and X. R. Wu: Nucl. Phys. A524 (1991) 404
16. A. A. Raduta, A. Faessler and S. Stoica: Nucl. Phys. A534 (1991) 149
17. J. Toivanen and J. Suhonen: Phys. Rev. Lett. 75 (1995) 410
18. J. Suhonen, T. Taigel and A. Faessler: Nucl. Phys. A486 (1988) 91
19. A. Balysh et al.: Phys. Lett. B356 (1995) 450
20. M. Moe and P. Vogel: Ann. Rev. Nucl. Part. Sci. 44 (1994) 247
21. A. S. Barabash et al.: Phys. Lett. B345 (1995) 408
22. NEMO-3 Proposal. LAL preprint 94-29 (1994)
23. D. Dassié et al.: Nucl. Instr. Meth. A309 (1991) 465
24. R. Arnold et al.: Nucl. Instr. Meth. A354 (1995) 338
25. D. Dassié et al.: Phys. Rev. D51 (1995) 2090
26. P. Billoir: Nucl. Instr. Meth. A255 (1984) 352
27. I. Kisel, V. Neskoromnyi and G. Ososkov, Application of Neural Networks in Experimental Physics, Phys. Part. Nucl. 24 (6) (1993) 657.
28. R. Arnold et al.: JETP Letters 61 (1995) 170

29. O. Helene: Nucl. Instr. Meth. B212 (1983) 319; Particle Data Group, Phys. Rev. D 50 (1994) 1281; K. Hikasa et al., Phys. Rev. D 45 (1992) S1
30. F.A. Danevich et al.: Phys. Lett. B344 (1995) 72
31. H. Ejiri et al.: J. Phys. Soc. of Japan 64 (1995) 339
32. A. Piepke et al.: Nucl. Phys. A577 (1994) 493
33. T. Bernatowicz et al.: Phys. Rev. C47 (1993) 806
34. J.-C. Vuilleumier et al.: Phys. Rev. D48 (1993) 1009
35. M.E. Moe, M.A. Nelson and M.A. Vient: Prog. Part. Nucl. Phys. 32 (1994) 247
36. M. Beck et al.: Phys. Rev. Lett. 70 (1993) 2853
37. J. Suhonen and O. Civitarese: J. Phys. G: Nucl. Part. Phys. 20 (1994) 347
38. J.G. Hirsh et al.: Nucl. Phys. A 584 (1995) 124
39. O.K. Manuel, J. Phys. G17 (1991) 221.
40. N. Takaoka, Y.Motomura and K.Nagao, Phys. Rev. C53 (1996) 1557.

This article was processed by the author using the LaTeX style file *pljour2* from Springer-Verlag.